The Master Activator of IncA/C Conjugative Plasmids Stimulates Genomic Islands and Multidrug Resistance Dissemination

Nicolas Carraro[1][9], Dominick Matteau[2][9], Peng Luo[1,3], Sébastien Rodrigue[2]*, Vincent Burrus[1]*

1 Laboratory of bacterial molecular genetics, Département de biologie, Université de Sherbrooke, Sherbrooke, Canada, 2 Laboratory of microbial systems and synthetic biology, Département de biologie, Université de Sherbrooke, Sherbrooke, Canada, 3 CAS Key Laboratory of Tropical Marine Bio-resources and Ecology, South China Sea Institute of Oceanology, Chinese Academy of Sciences, Guangzhou, China

Abstract

Dissemination of antibiotic resistance genes occurs mostly by conjugation, which mediates DNA transfer between cells in direct contact. Conjugative plasmids of the IncA/C incompatibility group have become a substantial threat due to their broad host-range, the extended spectrum of antimicrobial resistance they confer, their prevalence in enteric bacteria and their very efficient spread by conjugation. However, their biology remains largely unexplored. Using the IncA/C conjugative plasmid pVCR94ΔX as a prototype, we have investigated the regulatory circuitry that governs IncA/C plasmids dissemination and found that the transcriptional activator complex AcaCD is essential for the expression of plasmid transfer genes. Using chromatin immunoprecipitation coupled with exonuclease digestion (ChIP-exo) and RNA sequencing (RNA-seq) approaches, we have identified the sequences recognized by AcaCD and characterized the AcaCD regulon. Data mining using the DNA motif recognized by AcaCD revealed potential AcaCD-binding sites upstream of genes involved in the intracellular mobility functions (recombination directionality factor and mobilization genes) in two widespread classes of genomic islands (GIs) phylogenetically unrelated to IncA/C plasmids. The first class, SGI1, confers and propagates multidrug resistance in *Salmonella enterica* and *Proteus mirabilis*, whereas MGI*Vmi*1 in *Vibrio mimicus* belongs to a previously uncharacterized class of GIs. We have demonstrated that through expression of AcaCD, IncA/C plasmids specifically trigger the excision and mobilization of the GIs at high frequencies. This study provides new evidence of the considerable impact of IncA/C plasmids on bacterial genome plasticity through their own mobility and the mobilization of genomic islands.

Introduction

Multidrug resistance (MDR) is steadily increasing in Gram-negative bacteria in both community and hospital settings, and represents a growing concern worldwide [1]. MDR usually results from the adaptation of microorganisms through various mutations or from the acquisition of foreign DNA by horizontal gene transfer. In recent years, conjugative plasmids of the IncA/C incompatibility group, which are prevalent in enteric bacteria, have become a substantial threat due to their broad host-range, their extended spectrum of antimicrobial resistance and their efficient spread by conjugation [2]. IncA/C plasmids were first identified more than 40 years ago from diseased fish infected by antibiotic-resistant *Aeromonas hydrophila* and *Vibrio* spp [3,4]. For more than three decades IncA/C plasmids received relatively little attention, but the rapid dissemination of these MDR-carrying vectors among enteric pathogens recovered from food-producing animals, food products and humans have sprung intensive research at the epidemiological and genomic level. Several IncA/C plasmids are spreading the New Delhi metallo-lactamase bla_{NDM-1} gene and its variants, which confer resistance to all β-lactams except for monobactams and are widely distributed throughout all Gammaproteobacteria [5–8]. Resistance to β-lactams, aminoglycosides, chloramphenicol, folate pathway inhibitors (sulfonamides and trimethoprim), quinolones and tetracycline is also commonly conferred by these large plasmids (ca. 140 to 200 kb) [9–13]. IncA/C plasmids have also been shown to mobilize in *trans* the *Salmonella* genomic island 1 (SGI1), a 43-kb chromosomal mobile element carrying a class 1 integron that confers resistance to ampicillin, chloramphenicol, streptomycin,

Author Summary

Multidrug resistance is a major health concern that complicates treatments of even the most common infections caused by bacteria. In recent years, IncA/C plasmids have emerged and spread in bacteria infecting humans, food-producing animals and food products, driving at the same time the dissemination of a broad spectrum of antibiotic resistance genes in environmental and in clinical settings. In this study, we have characterized the regulatory pathway that governs IncA/C plasmid dissemination. We have found that AcaCD, the master activator complex encoded by these plasmids, is not only essential for the dissemination of IncA/C plasmids but also activates unrelated mobile genetic elements in bacterial genomes, thereby further promoting the interspecies propagation of multidrug resistance and other adaptive traits at a very high frequency.

sulfonamides and tetracycline (ACSSuT phenotype) [14–16]. SGI1 and related MDR-conferring genomic islands (GIs) have been found in a large variety of *Salmonella enterica* serovars and in *Proteus mirabilis* [17]. To date, the genetic regulatory network and the nature of the interactions allowing the specific mobilization of SGI1 by IncA/C helper plasmids remain largely unknown.

Comparative genomics studies of IncA/C plasmids isolated from *Escherichia coli*, *S. enterica*, *Vibrio cholerae*, *Yersina pestis*, *Yersinia ruckeri*, *Klebsiella pneumoniae* and *Providencia stuartii* have revealed their close relationship [9,10,18,19]. IncA/C plasmids share a common core set of genes exhibiting more than 99% identity that is disrupted by antibiotic-resistance conferring cassettes. While several of these conserved genes are involved in conjugative transfer (*tra* genes) and replication (*repA*), most have unknown functions. IncA/C plasmids are distantly related to the integrative and conjugative elements (ICEs) of the SXT/R391 family, which are also broadly distributed among several species of *Enterobacteriaceae* and *Vibrionaceae* [10,19,20]. Although many IncA/C plasmids have been fully sequenced to date, little is known about their basic biology, and most importantly about the regulation of their dissemination by conjugation.

Previously, we have identified and characterized the IncA/C conjugative plasmid pVCR94 from the epidemic isolate *V. cholerae* O1 El Tor F1939 [19]. pVCR94 transfers at very high frequency (10^{-2} to 10^{-1}) across species and genera, and mediates resistance to co-trimoxazole, chloramphenicol, streptomycin, ampicillin and tetracycline [19]. Here, we have characterized the regulatory mechanisms that control the conjugative transfer function of IncA/C plasmids. Two transcriptional repressors, *acr1* and *acr2*, were shown to repress the expression of two plasmid-encoded conserved genes, *acaC* and *acaD*, that are essential for the activation of IncA/C *tra* gene expression. Chromatin immunoprecipitation coupled to exonuclease digestion (ChIP-exo) and RNA sequencing (RNA-seq) assays were used to characterize the AcaCD regulon. Finally, bioinformatics analyses and experimental evidence revealed that the AcaCD regulon expands beyond IncA/C plasmid-borne genes to include GIs such as SGI1 and another unrelated GI of *Vibrio mimicus*. Altogether these results reveal a mechanism by which IncA/C conjugative plasmids play a role more important than previously estimated in bacterial genome dynamics.

Results and Discussion

Identification of repressors of IncA/C plasmids transfer

Comparative genomics previously revealed a set of six genes coding for putative transcriptional regulators in pVCR94 that are also conserved in nearly all IncA/C plasmids [19] (Table S1). To determine whether these genes are involved in the regulation of pVCR94 transfer, we constructed in-frame deletions and tested the ability of the resulting mutants to transfer by conjugation. For convenience, we carried out all of our assays using the 120,572-bp pVCR94ΔX mutant (referred to as pVCR94 in the rest of the paper), in which a single cluster containing all antibiotic resistance genes except for *sul2* conferring resistance to sulfamethoxazole has been deleted [19]. Deletion of *vcrx025*, which codes for a putative HUβ-like DNA-binding protein, had no effect on plasmid transfer (3.94×10^{-3} exconjugant/donor for pVCR94Δ*vcrx025* compared to 3.51×10^{-3} exconjugant/donor for wild-type, $P = 0.4400$, two-tailed Student's *t*-test). Despite several attempts, we were unable to delete *vcrx027*, which codes for a Cro-like transcriptional regulator, suggesting that its absence is lethal. The adjacent gene *vcrx028* is predicted to code for a toxin protein (addiction module killer protein, IPR009241), suggesting that the co-transcribed gene *vcrx027* encodes its cognate antitoxin (see Dataset S1).

The remaining four putative regulator genes cluster near the origin of transfer (*oriT*) (Figure 1A). Deletion of either *vcrx146* (*acr1*), which codes for a putative Ner-like DNA-binding protein, or *vcrx150* (*acr2*), which codes for a predicted H-NS-like DNA-binding protein, resulted in a 23- and 5.6-fold increase of the frequency of transfer, respectively, thereby suggesting that both genes code for repressors of pVCR94 transfer (Figure 1B). For this reason, *vcrx146* and *vcrx150* were renamed *acr1* and *acr2*, for IncA/C repressors 1 and 2, respectively. Complementation of the Δ*acr1* and Δ*acr2* mutations by ectopic expression of the corresponding genes under control of an arabinose-inducible promoter (P_{BAD}) did not restore the wild-type transfer frequency (Figure 1B). However, overexpression of either *acr1* or *acr2* decreased transfer of wild-type pVCR94 by 14 and 3 fold, respectively. Since *acr1* is the first gene of an operon structure (see Dataset S1) containing the putative transcriptional activator genes *vcrx148* (*acaD*) and *vcrx149* (*acaC*) (see below), we tested whether *acr1* or *acr2* are able to repress expression from P_{acr1}, the promoter driving expression of the operon containing *acr1* (Figure 1A). To do this, we cloned P_{acr1} upstream of a promoterless *lacZ* gene and monitored the β-galactosidase activity upon expression of *acr1* or *acr2* driven by P_{BAD}. While P_{acr1} was transcriptionally active in the absence of arabinose, no β-galactosidase activity was detected upon expression of either *acr1* or *acr2*, confirming that both proteins are capable of directly repressing expression from P_{acr1} (Figure 1C).

AcaC and AcaD are key activators of IncA/C plasmids transfer

The cluster of genes *acr1-vcrx147-acaDC-acr2* is extremely well conserved and remain syntenic among all IncA/C plasmids except for XCN1_p from *Xenorhabdus nematophila* in which it is completely absent (Figures 2 and S1). Interestingly, the IncA/C plasmids pAM04528 and pSN254 from *S. enterica*, which were reported to be non-self-transferable [10,21,22], code for a truncated AcaC protein resulting from a frameshift mutation (*acaC263*) (Figure 2), suggesting a key role of *acaC* in the activation of IncA/C-plasmid transfer. Unfortunately, no data is currently available about the intercellular mobility of five other plasmids coding for truncated AcaC or AcaD proteins (Figure 2) [23,24]. However, pRA1 was reported to transfer at a frequency of
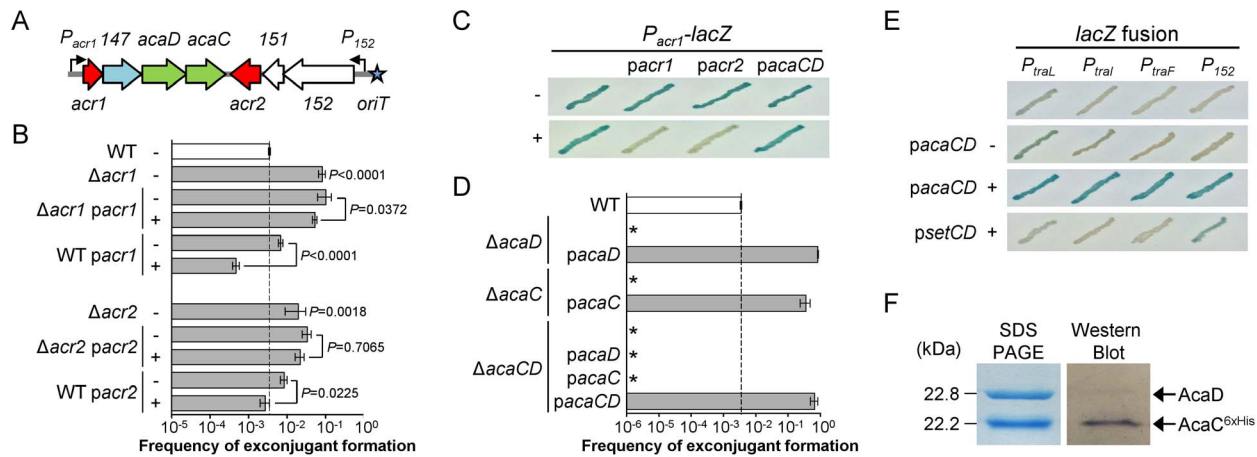
Figure 1. Regulation of IncA/C plasmids. (A) Schematic representation of the regulatory region of IncA/C plasmids. Genes and promoters are represented by arrowed boxes and angled arrows, respectively. Repressors and activators are shown in red and green, respectively. Genes of unknown function are shown in white and the gene coding for a putative lytic transglycosylase is shown in light blue. Locus names vcrxXXX are abbreviated as XXX. The oriT locus is depicted by a blue star. (B) Effect of the deletion and the overexpression of the negative transcriptional regulator-encoding genes acr1 and acr2. Conjugation assays were carried out using as donors E. coli BW25113 Nx containing pVCR94ΔX2 (WT) or its Δacr1 and Δacr2 mutants. Complementation and overexpression assays were performed with (+) or without (−) arabinose for the expression of acr1 (pacr1) or acr2 (pacr2) from the inducible P_{BAD} promoter. E. coli MG1655 Rf was used as the recipient. Transfer frequencies are expressed as a number of exconjugant per recipient CFUs. The bars represent the mean and standard deviation values obtained from at least three independent experiments. Statistical analyses were performed on the logarithm value of the means using one-way ANOVA with Tukey's multiple comparison test. P-values are indicated next to the bars when comparison referred to WT or next to the brackets when comparing two bars. (C) The constitutive promoter of acr1 (P_{acr1}) is repressed by Acr1 and Acr2. Activity of P_{acr1} was monitored from a single-copy, chromosomally integrated lacZ transcriptional fusion (P_{acr1}-lacZ). Colorimetric assays were carried out on LB medium supplemented with 40 µg/ml of X-Gal and induction with (+) or without (−) arabinose to express acr1, acr2 or acaCD from P_{BAD} on pacr1, pacr2 or pacaCD, respectively. (D) AcaC and AcaD are essential for conjugative transfer. Transfer assays were carried out using E. coli BW25113 Nx containing pVCR94ΔX2 (WT) or the mutants ΔacaC, ΔacaD or ΔacaCD. Complementation assays were performed by expressing acaC, acaD or acaCD from P_{BAD} on pacaC, pacaD and pacaCD, respectively. Recipient strains and statistical analyses were as described for panel B. All P-values are below 0.0001 when compared to the WT. The asterisk indicates that frequency of exconjugant formation was below the detection limit (<10^{-8}). (E) AcaCD is the direct activator of tra gene promoters. Activity of the P_{traL}, P_{traI}, P_{traF} and P_{152} was monitored from single-copy, chromosomally integrated lacZ transcriptional fusions. Colorimetric assays were performed as described in panel C with expression of acaCD or setCD from P_{BAD} on pacaCD or psetCD (pGG2B), respectively. (F) AcaD co-purifies with AcaC. Coomassie blue-stained SDS-PAGE and Western blot analysis of AcaC purified using a Ni-NTA affinity chromatography. AcaD and 6×His-tagged AcaC were co-expressed in E. coli BL21(DE3) from pacaDC$^{6×His}$. Western blot analysis was performed using a monoclonal antibody against the 6×His-tag.
doi:10.1371/journal.pgen.1004714.g001

10^{-3} [9] despite a GTG insertion at the 3′ end of acaC (acaC523ΩGTG) that slightly alters the primary sequence of AcaC C-terminus (Figure 2).

Pfam analyses (database v27.0) revealed that the conserved gene products AcaC and AcaD exhibit weak homology with the FlhC (Pfam PF05280) and FlhD (PF05247) domains, respectively (Table S1) [19]. FlhC and FlhD form a heteromeric complex playing a key role in the transcriptional activation of flagellar genes in Gram-negative bacteria such as E. coli [25]. We thus hypothesized that AcaC and AcaD (IncA/C activator subunits C and D) could acts as the master activator of tra genes in IncA/C plasmids. We constructed three null mutants, ΔacaC, ΔacaD and ΔacaCD, of pVCR94 and tested their ability to transfer by conjugation. All three mutations abolished conjugative transfer, thereby confirming that acaCD plays an essential role for IncA/C plasmid transmission (Figure 1D). Trans-complementation of these mutations under control of P_{BAD} restored and even outperformed transfer of pVCR94 (Figure 1D). Importantly, the ΔacaCD mutant could not be complemented by expression of either acaC or acaD. Only the simultaneous expression of both acaC and acaD restored the transfer of pVCR94ΔacaCD, strongly suggesting that these two genes code for an FlhCD-like activating complex (Figure 1D). AcaC and AcaD share 34% and 23% identity with the master activator subunits SetC and SetD encoded by SXT/R391 ICEs. As expected from the very poor percentage of identity, the

ΔacaCD mutation was not complemented by setCD expressed from the IPTG-inducible promoter P_{tac} (Figure S2).

To test whether AcaCD is necessary and sufficient to drive the expression of tra genes of pVCR94, we cloned the promoter regions of traL (P_{traL}), traI (P_{traI}) and traF (P_{traF}) upstream of a promoterless lacZ gene. The genes traL, traI and traF are likely candidate for AcaCD activation as traI codes for the predicted relaxase that would initiate conjugative transfer of pVCR94 at oriT while traL and traF code for two predicted sex pilus assembly proteins. We also tested the promoters P_{acr1} and P_{152} that drive the expression of acaCD and vcrx152, respectively (Figure 1A). All but P_{acr1} were inactive in the absence of acaCD, without arabinose induction or upon expression of setCD (Figure 1C, E). The constitutive expression from P_{acr1} seemed to remain unaffected by AcaCD overexpression. In contrast, expression of AcaCD alone in cells lacking pVCR94 was sufficient to trigger the expression from P_{traL}, P_{traI}, P_{traF} and P_{152} (Figure 1E).

Collectively, these results are consistent with a model in which acr1 represses acaCD expression and its own, thereby preventing expression of the tra genes. Accordingly, under the appropriate conditions, repression by Acr1 would be alleviated, allowing expression of acaCD that in turn would enable expression of the tra genes and other genes such as vcrx152. Although acr2 seems to be part of the same operon-like structure as vcrx152, its expression is not up-regulated by AcaCD and likely not driven by P_{152}
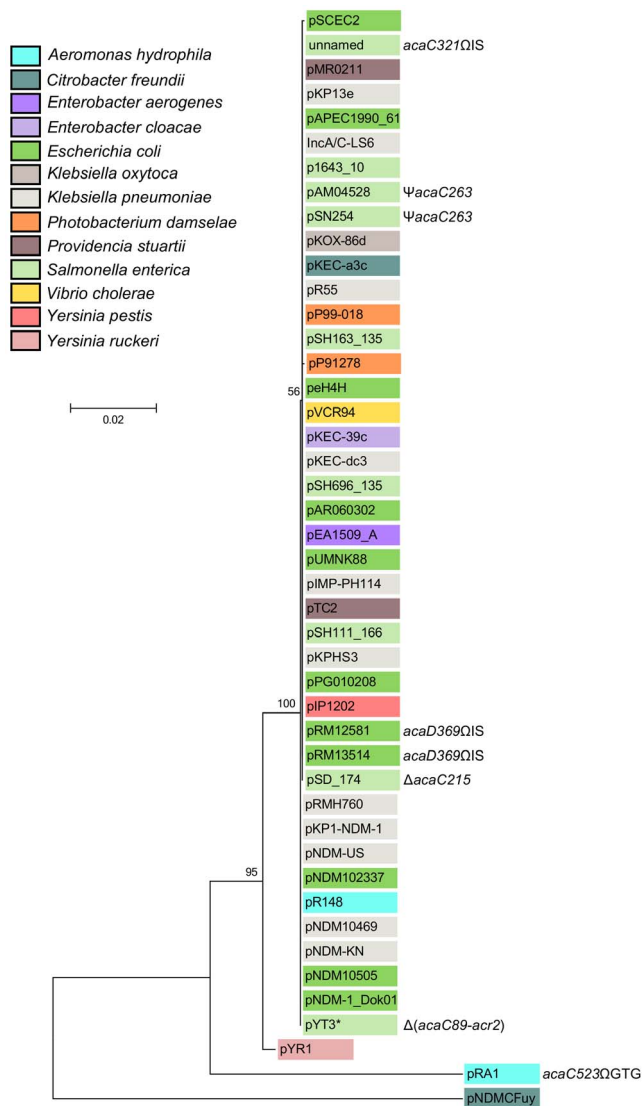
Figure 2. Molecular phylogenetic analysis of the *acr1-vcr147-acaDC-acr2* locus by Maximum Likelihood method. The evolutionary history was inferred by using the Maximum Likelihood method based on the Kimura 2-parameter model [61]. The tree with the highest log likelihood (−5461.6977) is shown. The percentage of trees in which the associated taxa clustered together is shown next to the branches. A discrete Gamma distribution was used to model evolutionary rate differences among sites (5 categories (+G, parameter = 0.6567)). The tree is drawn to scale, with branch lengths measured in the number of substitutions per site. The analysis involved 45 nucleotide sequences (Table S2). Codon positions included were 1st+2nd+3rd+Noncoding. There were a total of 2469 positions in the final dataset. Evolutionary analyses were conducted in MEGA6 [58]. The background color of each leaf indicates the original host species from which each plasmid was isolated. Insertions (Ω), deletion (Δ) and frameshift (Ψ) mutations are indicated where appropriate. *, Although pYT3 shares sequence identity with the IncA/C plasmids, it lacks an IncA/C-specific replication initiation gene (*repA*) and contains an IncFIB replicon instead (Figure S1) [62].

(Dataset S1). Instead *acr2* seems to be constitutively expressed. As a mild H-NS-like general repressor, Acr2 could dampen *acr1* and *acaCD* expression to prevent overexpression of the conjugative machinery, which is likely deleterious to the fitness of the host [26].

The H-NS-like protein Sfh encoded by the IncHI1 conjugative plasmid R27 has been shown to provide a stealth function helping the transmission of R27 into a naïve host by preventing titration of the cellular pool of H-NS by the A+T-rich sequences of the plasmid [27]. The locus occupied by *acr2* in IncA/C plasmids contains the gene *int* in the SXT/R391 ICEs (Figure S3) [20]. *int* codes for the integrase which allows SXT/R391 ICEs to remain quiescent in the host chromosome [28].

Although the regulation loci of IncA/C conjugative plasmids and SXT/R391 ICEs encode similar transcriptional activators (AcaCD and SetCD, respectively), IncA/C plasmids carry *acr1* and an extra *acr2* gene, while lacking a homolog of *setR* (Figure S3). In SXT/R391 ICEs, *setR* codes for a λ CI-related transcriptional repressor that prevents the expression of *setC* and *setD* [29,30]. Like λ CI, SetR responds to DNA damage by RecA*-dependent autoproteolysis, which alleviates the repression of *setCD*, thereby allowing excision and transfer of SXT/R391 ICEs [30]. Consistent with the absence of a *setR* homolog, transfer of IncA/C plasmids has been shown to be *recA*-independent [19].

AcaC and AcaD assemble as a heteromeric activator complex

Because deletion of either *acaC* or *acaD* abolished pVCR94 transfer, and both mutations could be individually complemented in *trans*, we sought to test whether AcaC and AcaD could form a heteromeric transcriptional activator complex. To investigate this possibility, we constructed a C-terminally 6×His-tagged version of *acaC*, *acaC*$^{6×His}$ that was expressed together with *acaD* from P_{tac}. AcaC$^{6×His}$ was purified by Ni-NTA affinity chromatography and the sample was analyzed on a 12% SDS-polyacrylamide gel. Interestingly, two bands were detected after Coomassie blue staining with molecular weights consistent with AcaC and AcaD (Figure 1F). Western blot assays using anti-6×His-tag antibodies only revealed the smallest 22.2-kDa band which corresponds to AcaC$^{6×His}$. The additional band that co-purified with AcaC$^{6×His}$ has a molecular weight of 22.8 kDa and was confirmed to be AcaD by mass spectrometry. Therefore, our results suggest that, like FlhC and FlhD, AcaC and AcaD assemble as a heteromeric complex.

Identification of AcaCD targets in pVCR94

To get a better understanding of the mechanisms governing transfer regulation of IncA/C conjugative plasmids, and identify genes of pVCR94 expressed under the direct control of AcaCD, we undertook an exhaustive characterization of the AcaCD regulon using transcriptome sequencing and ChIP-exo [31]. For these experiments, we used *E. coli* MG1655 Rf carrying pVCR94Δ*acaCD* and the same strain bearing a chromosomally integrated single copy of p*acaDC*$^{3×FLAG}$ that expresses the native AcaD subunit along with a C-terminal 3×FLAG tagged AcaC subunit under control of P_{tac}. Based on the transfer frequency of the Δ*acaCD* mutant complemented with *acaDC*$^{3×FLAG}$, we concluded that the 3×FLAG did not significantly affect the function of the tagged AcaC subunit compared to its wild-type counterpart (Figure S2).

ChIP-exo data analyses revealed 17 major AcaCD enrichment peaks, all located within intergenic regions (Figure 3A, B and Table S3). Most of the genes or operons found downstream of these peaks play key roles in conjugative transfer (Figure 3, Figure S4 and Table S3). For instance, AcaCD-binding sites were found upstream of the *traL*, *traV*, *dsbC*, *traN* and *traF* genes that are predicted to be involved in the formation of the mating pore. One peak was also found upstream of the gene coding for the putative relaxase gene *traI*. The presence of an AcaCD-binding site is also
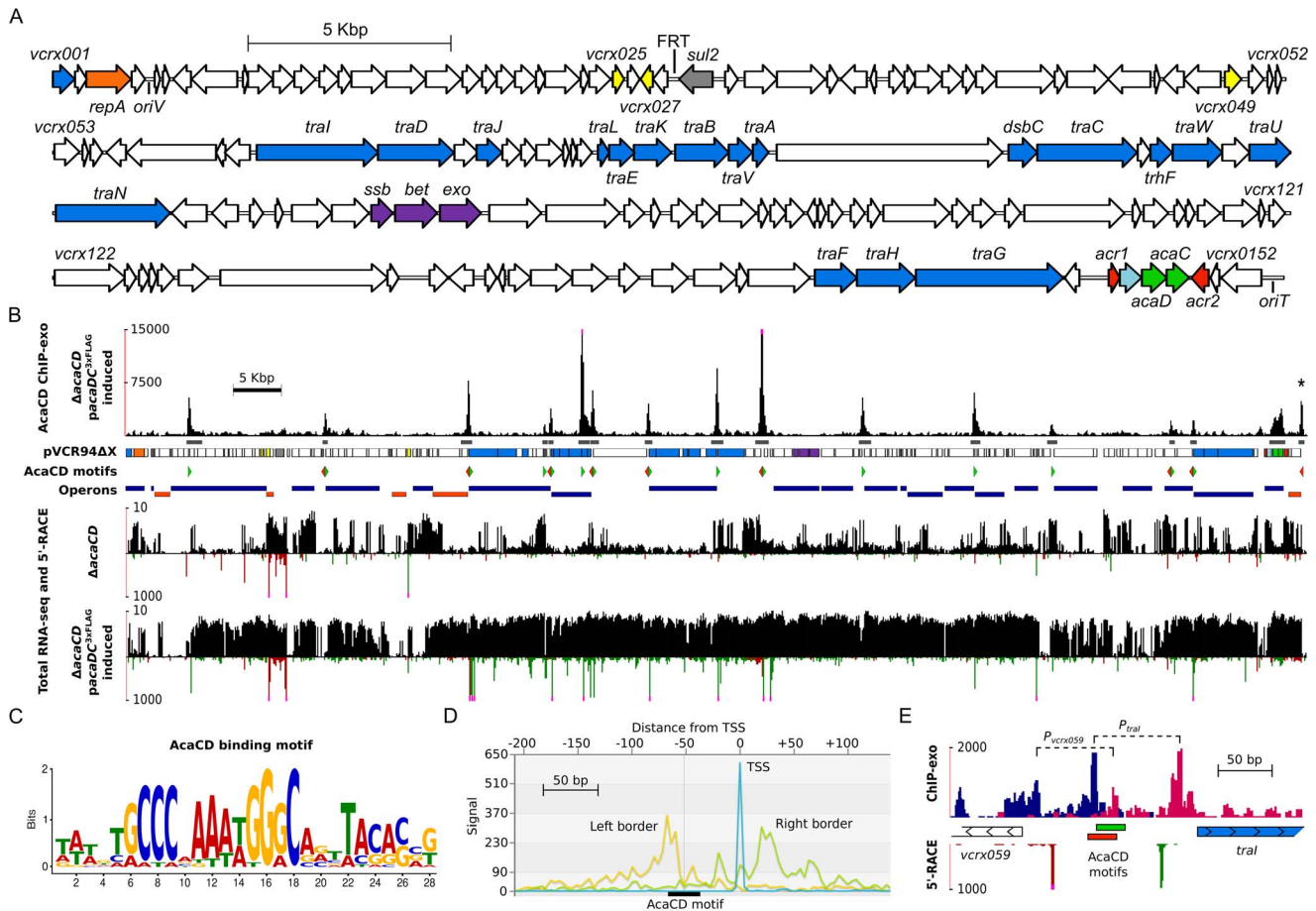
Figure 3. In-depth analysis of the AcaCD regulon in pVCR94. (A) Genetic organization of pVCR94ΔX adapted from Carraro *et al.* [19]. The circular map of the plasmid was linearized at the start position of gene *vcrx001*. The locations and orientations of ORFs are indicated by arrowed boxes. Colors are coded by function as follow: white, unknown; blue, conjugative transfer; light blue, lytic transglycosylase; orange, replication; gray, antibiotic resistance; yellow, putative regulatory function; purple, recombination; green, activator; red, repressor. The origin of replication (*oriV*) and the origin of transfer (*oriT*) are also indicated. The position of the scar resulting from the deletion of the antibiotic resistance gene cluster is indicated by FRT. *sul2*, resistance to sulfamethoxazole. (B) Results of ChIP-exo and RNA-seq experiments on *E. coli* MG1655 Rf carrying pVCR94ΔacaCD with or without a single chromosomal copy of pacaDC$^{3×FLAG}$ expressing the native AcaD subunit along with a C-terminal 3×FLAG-tagged AcaC subunit induced by IPTG. The first track plots the number of ChIP-exo reads mapped as a function of the position in pVCR94ΔX (black bars). Pink dots at the top of peaks indicate a signal beyond the represented y-axis maximal value. The second track shows the position of ChIP-exo enrichment peaks found by MACS [63] (dark gray). The asterisk at the top of the rightmost peak indicates a MACS false negative result manually incorporated in the figure. The third track is a representation of the pVCR94ΔX genes using the same color code as in panel A. The fourth track indicates the position of the AcaCD-binding motifs found by MAST [64] within ChIP-exo peaks using the AcaCD logo shown in panel C. Green arrows, motifs on positive DNA strand; red arrows, motifs on negative DNA strand. The fifth track represents Rockhopper's [65] predicted operons. Dark blue, operons transcribed from positive DNA strand; orange, operons transcribed from negative DNA strand. The remaining four tracks show the total RNA-seq read densities (black bars; log scale) and the genome-wide 5′-RACE signals (green and red bars respectively on the positive and negative DNA strands; linear scale) for cells harboring either pVCR94ΔacaCD or pVCR94ΔacaCD complemented with pacaDC$^{3×FLAG}$ and induced by IPTG. Pink dots at the top of 5′-RACE signals indicate a signal beyond the represented y-axis maximal value. (C) Motif sequence recognized by AcaCD in pVCR94ΔX obtained by MEME [64] using the AcaCD-binding sequences generated from ChIP-exo experiments. (D) VAP aggregate profile [66] showing ChIP-exo and 5′-RACE density signals centered on the AcaCD-binding motif (black box). Yellow line, density of reads mapping on the positive DNA strand (Left border); green line, density of reads mapping on the negative DNA strand (Right border). X-axis displays the distance in nucleotides from the aggregated transcription start site shown in blue (TSS). (E) Organization of *vcrx059* and *traI* divergent promoters revealed by ChIP-exo and 5′-RACE for pVCR94ΔacaCD complemented with IPTG-induced pacaDC$^{3×FLAG}$. The first track plots ChIP-exo read densities at single nucleotide resolution as in panel D. Dark blue, density of reads mapping on the positive DNA strand; magenta, density of reads mapping on the negative DNA strand. The second track shows the two AcaCD-binding motifs found by MAST within the ChIP-exo peak between *vcrx059* (white arrows) and *traI* (blue arrows) genes. Motif corresponding to the positive DNA strand is represented in green and motif corresponding to the negative DNA strand is shown in red. The last track represents 5′-RACE signals as described in panel B. The exonuclease-protected regions of the *vcrx059* and *traI* promoters are indicated by dashed lines.

doi:10.1371/journal.pgen.1004714.g003

well correlated with transcriptional activity since the expression of 86 out of 152 genes, including genes located downstream of AcaCD-binding sites, is clearly increased under the same conditions used for ChIP-exo when compared to a ΔacaCD mutant (Figure 3B and Dataset S1). In contrast, the vast majority of genes that are not significantly affected by the expression of AcaCD appeared to be either inactive or likely constitutively expressed. Their function is unknown or not directly tied to conjugative transfer. Examples of such genes in pVCR94 include *repA* (*vcrx003*) involved in plasmid replication, a putative

toxin-antitoxin system (*vcrx028* and *vcrx027*), the *sul2* (*vcrx029*) gene conferring resistance to sulfamethoxazole, as well as *acr1* and *acr2* that negatively regulate the expression of the *acr1-vcrx147-acaDC* operon (Figure 1A, C and Dataset S1).

De novo motif discovery of DNA sequences bound by AcaCD was carried out using MEME (Multiple Em for Motif Elicitation) [32] (Figure 3C). We next used MAST (Motif Alignment and Search Tool) [33] to determine the precise location of potential AcaCD-binding motifs on the entire sequence of pVCR94 (Figure 3B, Figure S4, and Table S3). Statistically significant motifs that were localized within ChIP-exo peaks were conserved. We next analyzed the localization of AcaCD-binding motifs relative to transcription start sites obtained using a genome-wide 5′-RACE (Rapid Amplification of cDNA Ends) methodology (Figure 3B, D, Figure S4 and Table S3). We observed a similar promoter profile, compatible with a class 2 activator [34], for all transcription start sites located between an AcaCD-binding motif and a gene in the same orientation (Figure S4). This interpretation is consistent with our high resolution ChIP-exo data that reveals a protected region containing a distal AcaCD motif (Figure 3D), and supported by previous observations of the promoter-bound RNA polymerase holoenzyme complex footprint between position −54 to +22 relative to the transcription start site [28]. An interesting example of this organization is the regulation of the *vcrx059* and *traI* divergent promoter region, in which two partially overlapping transcription initiation complexes are detected (Figure 3E).

In addition to measuring transcriptome expression in pVCR94Δ*acaD* and pVCR94Δ*acaCD* complemented with IPTG-induced p*acaDC*$^{3×FLAG}$, we also performed RNA-seq on wild-type pVCR94 (Dataset S1). Our results indicate little differences between the transcriptome expression levels of wild-type pVCR94 and p*acaDC*$^{3×FLAG}$-complemented pVCR94Δ*acaCD* (Pearson coefficient of 0.87). On the contrary, these two transcriptomes are clearly different from pVCR94Δ*acaCD* (Pearson coefficients of 0.12 and −0.04, respectively). In total, pVCR94 and p*acaDC*$^{3×FLAG}$-complemented pVCR94Δ*acaCD* share 76 differentially expressed genes out of 88 when compared to pVCR94Δ*acaCD*, which further supports the high similarity between their gene expression profiles (Dataset S1). These findings suggest that AcaCD in wild-type pVCR94 is at least partially active in *E. coli* under laboratory conditions because an appropriate activating signal is already being sensed and/or the expression of *acaC* and *acaD* is not efficiently repressed. This hypothesis is consistent with the fact that *acr1* and *acr2* negatively regulate conjugative transfer efficiency while not completely abolishing it (Figure 1B). Our results strikingly contrast with the conclusion drawn by others that most of the backbone of IncA/C plasmid pAR060302, including *tra* genes, is transcriptionally inactive in *E. coli* [35]. This interpretation is puzzling given the very high nucleotide identity between core regions of IncA/C plasmids, that reads per kilobase per million reads (RPKM) expression values reported for pAR060302 genes expressed at a "low level" such as *repA* reach several thousand units [35], and that pAR060302 is self-transferable at high frequencies by conjugation under laboratory conditions similar to ours [22].

AcaCD drives the mobility of two unrelated classes of genomic islands
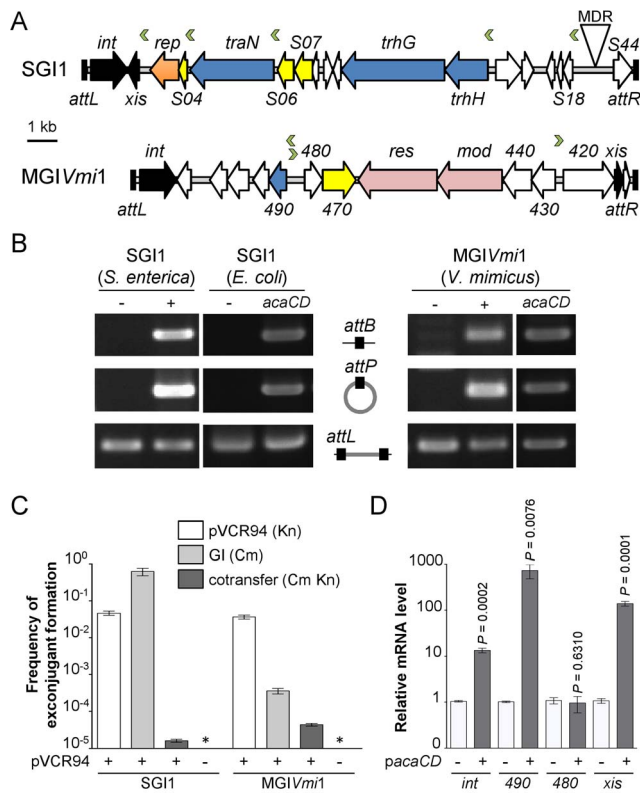
Determination of the AcaCD-bound DNA motif provides the opportunity to investigate the impact of IncA/C plasmids on genome dynamics. For instance, IncA/C plasmids are known to mobilize SGI1 in *S. enterica* by a yet uncharacterized mechanism [14,15,36]. SGI1 elements confer and propagate MDR in various pathogenic bacteria [16,17,37]. Data mining using the

AcaCD-binding motif revealed putative sites upstream of the genes *xis*, *S004/rep*, *traN* and *trhH/trhG* likely involved in the mobility (recombination directionality factor and mobilization genes) of SGI1 (Figure 4A and Table 1). We carried out a similar analysis on the sequenced genome of *V. mimicus* VM573 and identified three AcaCD-binding motifs upstream of three genes, two of which coding for a predicted recombination directionality factor (VMD_06410, *xis*) and a distant homolog of Vcrx001 (VMD_06490, 29% of identity over 85 amino acid residues), which is a conserved key factor for conjugative transfer of IncA/C plasmids (Table 1) [19]. The third gene, VMD_06480, has no predicted function. The three genes are part of an unannotated 16 511-bp GI integrated into the 3′ end of *yicC*, that we named MGI*Vmi*1 (Figure 4A and Table 1). MGI*Vmi*1 could confer adaptive traits to its host, notably resistance to bacteriophages conferred by a putative type III restriction-modification (*res-mod*) (Figure 4A). SGI1 and MGI*Vmi*1 are prototypes of two families of GIs that are phylogenetically unrelated to each other and to IncA/C plasmids.

Based on these observations, we hypothesized that expression of *acaCD* either from pVCR94 or from pBAD30 would trigger the excision of both SGI1 and MGI*Vmi*1 from their respective host chromosome. To verify this hypothesis, we monitored by PCR amplification the formation of a chromosomal *attB* site and of an *attP* site resulting from the circularization of the two GIs (Figure 4B). While no spontaneous excision of either GI was detected in the absence of pVCR94, both GIs excised from the chromosome not only in the presence of pVCR94 but also upon ectopic expression of *acaCD* in cells lacking pVCR94 (Figure 4B). Finally, to confirm that IncA/C plasmids can mobilize the novel GI MGI*Vmi*1, we carried out inter- and intraspecific mating assays using pVCR94 as the helper plasmid and a modified MGI*Vmi*1 carrying *res::cat* (Cm resistant) as a selectable marker. As a positive control, we used SGI1 and took advantage of its natural selectable markers. For both SGI1 and MGI*Vmi*1, no exconjugant were observed in the absence of pVCR94 (Figure 4C). In contrast, both elements were specifically mobilized in its presence. On one hand, transfer of SGI1 occurred at very high frequency (almost all recipient cells received a copy of SGI1), but co-acquisition of pVCR94 was infrequent. This observation suggests that negative interactions may exist between these mobile genetic elements. On the other hand, MGI*Vmi*1 transferred at a lower rate than pVCR94 (Figure 4C). We confirmed AcaCD-specific expression of the MGI*Vmi*1-borne genes *xis* and VMD_06490 by real-time-quantitative PCR (RT-qPCR) (Figure 4D). *int* mRNA level was also specifically increased by AcaCD, despite the lack of a predicted AcaCD-binding motif in its promoter region. This observation suggests that its enhanced expression could be driven by the promoter upstream of *xis* on a large transcript containing *attP* on the circular excised form of MGI*Vmi*1. For a reason that remains to be established and despite the presence of a predicted AcaCD-binding motif, VMD_06480 expression was not regulated by AcaCD.

Unlike SGI1, which seem to encode a large set of proteins likely dedicated to mobilization (TraN, TrhG and TrhH), MGI*Vmi*1 only encodes a distant homolog of Vcrx001 (VMD_06490), which is strongly induced by AcaCD (Figure 4D). Based on these differences, we speculate that MGI*Vmi*1 is not as efficient as SGI1 to hijack the conjugative apparatus encoded by IncA/C plasmids. Characterization of the genetic and molecular mechanisms of SGI1 and MGI*Vmi*1 mobilization by IncA/C helper plasmids are ongoing.

Altogether, these results unraveled a novel example of the multiple and intricate interactions linking phylogenetically unre-

A

SGI1: int, rep, traN, S07, trhG, MDR S44
attL xis S04 S06 trhH S18 attR

1 kb

MGIVmi1: int 480 res mod 440 420 xis
attL 490 470 430 attR

B

SGI1 (*S. enterica*) | SGI1 (*E. coli*) | MGIVmi1 (*V. mimicus*)
− + | − acaCD | − + acaCD

attB
attP
attL

C

□ pVCR94 (Kn)
▨ GI (Cm)
■ cotransfer (Cm Kn)

Frequency of exconjugant formation

10^0
10^{-1}
10^{-2}
10^{-3}
10^{-4}
10^{-5}

pVCR94 + + + − | + + + −
SGI1 | MGIVmi1

D

Relative mRNA level

1000
100
10
1
0

$P = 0.0002$
$P = 0.0076$
$P = 0.6310$
$P = 0.0001$

pacaCD − + | − + | − + | − +
int | 490 | 480 | xis

Figure 4. IncA/C-dependent excision and transfer of GIs. (A) Schematic representation of SGI1 from *S. enterica* Typhimurium DT104 and MGIVmi1 from *V. mimicus* VM573. The left and right junctions (*attL* and *attR*) within the host chromosome are indicated. SGI1 (42 596 bp, Genbank AF261825) and MGIVmi1 (16 511 bp, Genbank NZ_A-CYV01000005) are integrated into the 3′ end of *trmE* and *yicC* (*attL* sides) in their respective hosts. ORFs with similar function are indicated by colors as follows: black, DNA recombination; orange, DNA replication; blue, conjugative transfer; yellow, regulatory function; pink, putative type III restriction-modification system; white, unknown functions; MDR, multidrug resistance locus. Green chevrons indicate the position and orientation of predicted AcaCD-binding sites (see Table 1). For clarity, ORF names *S0XX* were shortened as *SXX* for SGI1 and VMD_06XXX as XXX for MGIVmi1. (B) AcaCD induces SG1 and MGIVmi1 excision. Excision was detected by PCR on genomic DNA to specifically amplify the *attB* chromosomal site and the *attP* site resulting from the excision of the GIs in *S. enterica* Typhimurium or *E. coli* bearing SGI1 and *V. mimicus* bearing MGIVmi1. Integrated GIs were detected by amplification of the *attL* site. Assays were done in strains devoid of plasmid (−), bearing pVCR94ΔX3 (+) or only expressing *acaCD* (*acaCD*) from pacaDC$^{3\times FLAG}$ for assays in *E. coli* or pacaCD in *V. mimicus*. (C) Intraspecific mobilization of both GIs was assayed using *E. coli* MG1655 Rf bearing pVCR94ΔX3 and SGI1 or MGIVmi1 as a donor and the otherwise isogenic strain MG1655 Nx as a recipient. Exconjugants were selected for the acquisition of either GI, pVCR94ΔX3, and for cotransfer of both. Transfer frequencies are expressed as the number of exconjugant per donor CFUs. The bars represent the mean and standard deviation values obtained from three independent experiments. The asterisk indicates that the frequency of exconjugant formation was below the detection limit ($<10^{-8}$). (D) AcaCD induces the expression of the putative excision and mobilization genes of MGIVmi1. Relative mRNA levels of *int* (VMD_06510), *490* (VMD_06490), *480* (VMD_06480) and *xis* (VMD_06410) were measured by RT-qPCR assays on cDNA of *V. mimicus* VM573 devoid of plasmid (−) or expressing *acaCD* from pacaCD (+). The bars represent the mean and standard deviation values obtained from three independent experiments. Comparison between the strain expressing or not AcaCD were done using two-tailed Student's *t*-tests and the *P*-values are indicated above to the bars.
doi:10.1371/journal.pgen.1004714.g004

lated mobile genetic elements. Moreover, our study provides new evidence that many GIs are not defective for their propagation but rather mobilizable GIs, whose biology is just linked and perfectly adapted to other self-transmissible helper elements [15,38,39,40] (Figure 5).

Concluding remarks

IncA/C conjugative plasmids and SXT/R391 ICEs both rely on transcriptional activator complexes that are reminiscent of the FlhDC master activator of flagellar genes to enable expression of their *tra* genes. Nevertheless, AcaCD recognizes DNA motifs that are unrelated to the recognition motif of FlhDC [25]. Moreover, AcaCD and SetCD, the master activator of SXT/R391 ICEs, are not exchangeable and are thus expected to recognize completely unrelated DNA motifs. Our study revealed that the AcaCD regulon extends beyond the sole genes involved in the dissemination of IncA/C plasmids and that AcaCD acts as a beacon signaling the presence of a helper plasmid, allowing the propagation of two unrelated classes of GIs. Similarly, SetCD has been shown to trigger the excision of MGIs originating from various pathogenic *Vibrio* species [38,39,41], thereby suggesting that sequences bound by AcaCD- and SetCD-like activators can be easily mimicked by unrelated GIs to regulate their own gene expression. Clearly, our results and observations from others indicate that GIs are not necessarily defective or decaying mobile genetic elements, unable to propagate. Instead, most are likely quiescent parasites awaiting opportunities to hijack helper self-transmissible elements using diverse strategies [14,38,42]. Such intricate connections between various genetic elements support their major impact on the evolution of genomes and on the adaptation of bacteria to their environment, particularly in the current context of massive emergence of multidrug resistant pathogens worldwide. Ultimately, future research investigating the regulation of other mobile genetic elements relying on similar transcriptional activator complexes to regulate their own dissemination will unravel unforeseen regulatory networks linking self-transmissible and mobilizable elements.

Materials and Methods

Bacterial strains and bacterial conjugation assays

The bacterial strains used in this study are described in Table 2. The strains were routinely grown in Luria-Bertani (LB) broth at 37°C in an orbital shaker/incubator and were maintained at −80°C in LB broth containing 15% (vol/vol) glycerol. Antibiotics were used at the following concentrations: ampicillin (Ap), 100 μg/ml; chloramphenicol (Cm), 20 μg/ml for *E. coli*, 30 μg/ml for *S. enterica* and 10 μg/ml for *V. mimicus*; erythromycin (Em), 10 μg/ml; kanamycin (Kn), 50 μg/ml or 10 μg/ml for single copy integrants of pOPlacZ; nalidixic acid (Nx), 40 μg/ml; rifampicin (Rf) 50 μg/ml; spectinomycin (Sp), 50 μg/ml; streptomycin (Sm), 200 μg/ml; sulfamethoxazole (Su), 160 μg/ml; tetracycline (Tc), 12 μg/ml; trimethoprim (Tm), 32 μg/ml. Conjugation assays were performed as described elsewhere [19]. To induce expression from pBAD30 and from pAH56 in complementation assays, mating experiments were carried on LB agar plates supplemented with 0.02% L-arabinose or 0.1 mM isopropyl β-D-1-thiogalactopyranoside (IPTG), respectively.

Molecular biology methods

Genomic and plasmid DNA were prepared using the Wizard Genomic DNA Purification Kit (Promega) and EZ-10 Spin Column Plasmid DNA Minipreps Kit (Biobasic), respectively, according to manufacturer's instructions. All the enzymes used in

Table 1. Prediction of putative AcaCD-binding sites in SGI1 and MGI*Vmi*1.

Element	Strand	Start	End	*p*-value[a]	Matched Sequence[b]	Downstream gene(s)
SGI1	−	2016	2043	3.2e-10	**TTCGCGCCCTAAAAGGGCAGATCCAGAG**	*xis*
SGI1	−	3541	3568	1.2e-11	**TAGGTGCCCAAATAGGGCACTTCCAGAG**	*S004/rep*
SGI1	−	6444	6471	6.1e-06	**CGTATGCCGCAAAAGGGCAAATAGCGAT**	*traN*
SGI1	−	13484	13511	7.9e-09	**GGACTGCCCAAATTGGACAGTTTGGGAG**	*trhH/trhG*
SGI1	−	16360	16387	2.6e-12	**AATGTGCCCAAAAAGGGCCAATACAGCG**	*S018*
MGI*Vmi*1	+	6832	6859	1.7e-07	**AAAATGCCCAATCAGGACAGTTTGAGCG**	VMD_06480/06470
MGI*Vmi*1	−	6827	6854	7.8e-06	**AAACTGTCCTGATTGGGCATTTTCGCAG**	VMD_06490
MGI*Vmi*1	+	15770	15797	2.4e-06	**TTCAGTACCAAAATGGGCAATTACAGAT**	VMD_06420/*xis*

[a]Only output matches with *p*-values below 1.0e-05 are shown and considered as significant hits.
[b]Matches were predicted by FIMO (MEME suite) based on the AcaCD logo presented in Figure 3C.
doi:10.1371/journal.pgen.1004714.t001
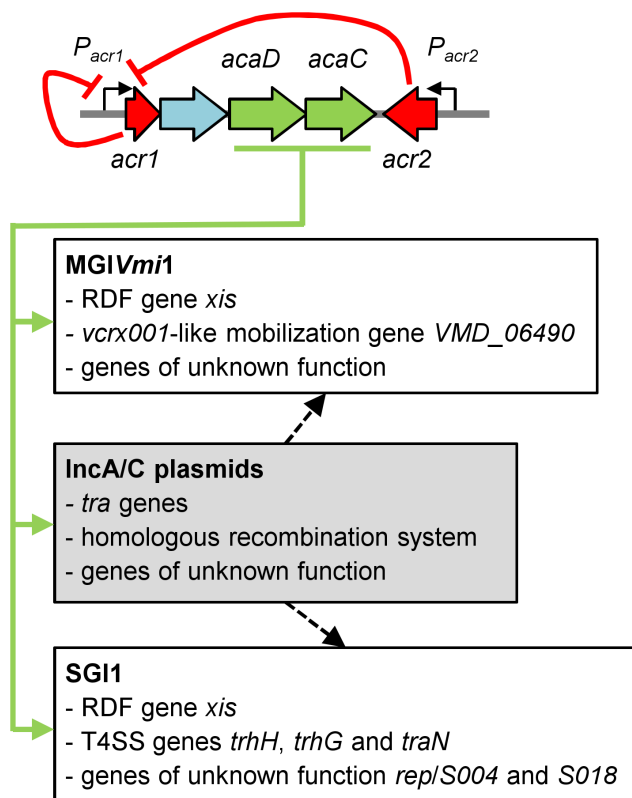
Figure 5. Model of regulation of IncA/C plasmids and interaction with genomic islands. Expression of the master activator complex AcaCD from the promoter of *acr1* (P_{acr1}) is directly repressed by Acr1 and Acr2 (red arrows). AcaCD directly activates the expression of the transfer genes of pVCR94, as well as the expression of the *bet/exo* homologous recombination system and numerous genes of unknown function (green arrows). AcaCD triggered the excision of SGI1 and MGI*Vmi*1 by directly activating the expression of the RDF genes *xis*. AcaCD activates the expression of the *vcrx001*-like mobilization gene and other genes of unknown function in MGI*Vmi*1. AcaCD also activates the expression of three genes coding for putative component of type IV secretion system (T4SS), as well as genes of unknown function such as *S004*, *rep* and *S018* in SGI1. IncA/C plasmids likely provide additional functions for genomic islands dissemination such as *oriT* recognition and processing or formation of the mating pore (black hatched arrows). Genes are color-coded as in Figure 1A.
doi:10.1371/journal.pgen.1004714.g005

this study were purchased from New England BioLabs or Enzymatics. PCR assays were performed with the primers described in Table S4. The PCR conditions were as follows: (i) 3 min at 94°C; (ii) 30 cycles of 30 sec at 94°C, 30 sec at the appropriate annealing temperature, and 1 minute/kb at 68°C; and (iii) 5 min at 68°C. When necessary, PCR products were purified using a EZ-10 Spin Column PCR Products Purification Kit (Biobasic) according to manufacturer's instructions. *E. coli* was transformed by electroporation according to Dower *et al*. [43]. *V. mimicus* was transformed by electroporation according to Occhino *et al*. [44] with modified G buffer (200 mM sucrose, 1 mM Hepes, pH 7.5). Electroporation was carried out in a BioRad GenePulser Xcell apparatus set at 25 µF, 200 V and 1.8 kV using 1-mm gap electroporation cuvettes. Sequencing reactions were performed by the Plateforme de Séquençage et de Génotypage du Centre de Recherche du CHUL (Québec, QC, Canada).

Plasmids and strains construction

Plasmids and oligonucleotides used in this study are listed in Table 2 and S4. Complementation vectors derived from the pBAD30 vector [45]. The ORFs *acr1*, *acr2*, *acaC*, *acaD* and *aca CD* were amplified using primers pairs vcrx146.for/vcrx146.rev, vcrx150.for/vcrx150.rev, vcrx149(acaC).for/vcrx149(acaC).rev, vcrx148(acaD).for/vcrx148(acaD).rev, vcrx148(acaD).for/vcrx149 (acaC).rev and cloned into the EcoRI restriction site of pBAD30 to generate p*acr1*, p*acr2*, p*acaC*, p*acaD* and p*acaCD*, respectively. The transcriptional fusion vector pOPlacZ contains the promoterless *lacZ* gene from *E. coli* K12 MG1655 with its native Shine-Dalgarno sequence. This plasmid was constructed by amplifying the *lacZ* gene using primer pair Op-lacZ-F/Op-lacZ-R and subsequent cloning into the 2 462-bp fragment of PstI-digested pAH56 using the Gibson assembly method [46]. PCR fragments containing the promoter region upstream of *acr1*, *traL*, *traI*, *traF* and *vcrx152* were cloned into the PstI restriction site of pOPlacZ to produce pProm*acr1*, pProm*traL*, pProm*traI*, pProm*traF* and pProm*152*, respectively. The vectors p*acaDC*$^{3×FLAG}$ and p*setDC*$^{3×FLAG}$ used for complementation assays and ChIP-exo experiments derived from pAH56. Briefly, the *acaDC* and *setDC* loci were amplified using primer pairs acaDF-NdeI/acaCR-HindIII and setDF-NdeI/setCR-HindIII, respectively, and cloned into pCR2.1 (Invitrogen) to generate pCR2.1::*acaDC* and pCR2.1::*setDC*. 3×FLAG was amplified from pJL148 [47] using the primer pair FlagF/FlagR and subsequently cloned into the HindIII site of pCR2.1::*acaDC* and pCR2.1::*setDC* to generate pCR2.1::*acaDC*$^{3×FLAG}$ and pCR2.1::*setDC*$^{3×FLAG}$. The *acaDC*$^{3×FLAG}$ and *setDC*$^{3×FLAG}$ inserts were recovered by NdeI/SalI

Table 2. Strains and plasmids used in this study.

Strains or plasmids	Relevant genotype or phenotype	References
Escherichia coli		
BW25113	F$^-$, Δ(araD-araB)567, ΔlacZ4787(::rrnB-3), λ–, rph-1, Δ(rhaD-rhaB)568, hsdR514	[50]
BW25113 Nx	Nx^r-derivative of BW25113	[19]
MG1655 Nx	Nx^r-derivative of MG1655	[51]
MG1655 Rf	Rf^r-derivative of MG1655	[51]
BL21(DE3)	F$^-$, ompT ΔhsdS gal dcm (DE3)	Novagen
β2163	(F$^-$) RP4-2-Tc::Mu ΔdapA::(erm-pir) (Kn Em)	[49]
Salmonella enterica		
St038	serovar Typhimurium; SGI1$^+$ (Ap Cm Tc Su Sp Sm)	F. Malouin
Vibrio mimicus		
VM573	Patient with diarrhea; USA, 1990s; CT$^+$ TCP$^+$ MGIVmi1$^+$ (Ap Sp Su)	[68]
Plasmids		
pVCR94	IncA/C conjugative plasmid; *V. cholerae* O1 F1939; Rwanda, 1994	[19]
pVCR94ΔX	Su^r-derivative of pVCR94 (Su)	[19]
pVCR94ΔX2	Sp^r-derivative of pVCR94ΔX (Sp Su)	This study
pVCR94ΔX3	Kn^r-derivative of pVCR94ΔX (Kn Su)	This study
pVCR94Δ25	pVCR94 ΔX2 Δvcrx025 (Sp Su)	This study
pVCR94ΔacaC	pVCR94 ΔX2 ΔacaC (Sp Su)	This study
pVCR94ΔacaD	pVCR94 ΔX2 ΔacaD (Sp Su)	This study
pVCR94ΔacaCD	pVCR94 ΔX2 ΔacaCD (Sp Su)	This study
pVCR94Δacr1	pVCR94 ΔX2 Δacr1 (Sp Su)	This study
pVCR94Δacr2	pVCR94 ΔX2 Δacr2 (Sp Su)	This study
pBAD30	ori$_{p15A}$ araC P$_{BAD}$ (Ap)	[45]
pacaC	pBAD30::acaC (Ap)	This study
pacaD	pBAD30::acaD (Ap)	This study
pacaCD	pBAD30::acaCD (Ap)	This study
pacr1	pBAD30::acr1 (Ap)	This study
pacr2	pBAD30::acr2 (Ap)	This study
pGG2B	pBAD30::setDC (Ap)	[69]
pSW23T	oriT$_{RP4}$; oriV$_{R6K\gamma}$ (Cm)	[49]
pAH56	oriV$_{R6K\gamma}$; attP$_\lambda$; lacI; P$_{tac}$ (Kn)	[70]
pJL148	SPA-tag (CBP-TEV site-3$\times$FLAG) (Kn)	[47]
pacaDC$^{3\times FLAG}$	pAH56::acaDC$^{3\times FLAG}$ (Kn)	This study
psetDC$^{3\times FLAG}$	pAH56::setDC$^{3\times FLAG}$ (Kn)	This study
pOPlacZ	pAH56 lacZ (Kn)	This study
pPromtraL	pOPlacZ P$_{traL}$-lacZ (Kn)	This study
pPromtraI	pOPlacZ P$_{traI}$-lacZ (Kn)	This study
pPromtraF	pOPlacZ P$_{traF}$-lacZ (Kn)	This study
pPromacr1	pOPlacZ P$_{acr1}$-lacZ (Kn)	This study
pProm152	pOPlacZ P$_{152}$-lacZ (Kn)	This study
pINT-ts	oriR101; cI857; λp_R-int$_\lambda$ (Ap Ts)	[70]
pET-24b(+)	oriV$_{pBR322}$; lacI; P$_{T7}$; 6$\times$His; expression vector (Kn)	Novagen
pacaDC$^{6\times His}$	pET-24b(+)::acaDC$^{6\times His}$ (Kn)	This study
pSIM6	λRed recombination thermo-inducible encoding plasmid (Ts Ap)	[52]
pKD3	PCR template for one-step chromosomal gene inactivation (Cm)	[50]
pKD13	PCR template for one-step chromosomal gene inactivation (Kn)	[50]
pVI36	PCR template for one-step chromosomal gene inactivation (Sp)	[51]

Table 2. Cont.

Strains or plasmids	Relevant genotype or phenotype	References
pCP20	Flp recombinase thermo-inducible encoding plasmid (Ts Ap Cm)	[53]

Ap, ampicillin; Cm, chloramphenicol; Em, erythromycin; Kn, kanamycin; Nx, nalidixic acid; Sp, spectinomycine; Rf, rifampicin; Sm, streptomycine; Su, sulfamethoxazole; Tc, tetracycline; Tm, trimethoprim; Ts, thermosensitive; CT, cholera toxin; TCP, toxin co-regulated pilus.
doi:10.1371/journal.pgen.1004714.t002

digestion and subsequently cloned into the NdeI/SalI-digested pAH56 to generate p$acaDC^{3\times FLAG}$ and p$setDC^{3\times FLAG}$ [48]. p$acaDC^{6\times His}$ was obtained by cloning of $acaDC$ amplified with acaDF-NdeI/acaCR-HindIII into pET-24b(+) (Novagen). pRes for insertion of a Cm marker into MGIVmi1 was obtained cloning into EcoRI/BamHI-digested pSW23T [49] the 732-bp PCR fragment amplified using the primer pair GIVmi-res2F/GIVmi-res2R on genomic DNA of *V. mimicus* VM573.

Deletion mutants of pVCR94ΔX were constructed using the one-step chromosomal gene inactivation technique and are listed in the Table 1 [19,50]. Primers used are listed in Table S4. The pVCR94ΔX derivatives pVCR94ΔX2 (Sp) and pVCR94ΔX3 (Kn) were constructed using primer pair 94DelXnoFRT.for/94DelXnoFRT.rev and pVI36 and pKD13 as templates, respectively [50,51]. Subsequent deletions of $vcrx025$, $acr1$, $acr2$, $acaC$, $acaD$ and $acaCD$ were done on pVCR94ΔX2 using primer pairs 94Delvcrx025.for/94Delvcrx025.rev, 94Delvcrx146.for/94Delvcrx146.rev, 94Delvcrx150.for/94Delvcrx150.rev, 94DelacaC.for/94DelacaC.rev, 94DelacaD.for/94DelacaD.rev and 94DelacaD.for/94DelacaC.rev, respectively, and pKD3 as the template. The λRed recombination system was expressed using pSIM6 as described by Datta *et al.* [52]. When possible, the antibiotic resistance cassette was removed from the resulting construction by Flp-catalyzed excision using the pCP20 vector [53]. All deletions were designed to be non-polar and verified by PCR and antibiotic resistance profiling.

MGIVmi1 was labelled with a Cm resistance marker in *V. mimicus* VM573 by inserting the pSW23T-derivative suicide plasmid pRes into the putative type III restriction gene *res*. Briefly, pRes was mobilized from *E. coli* β2163 to *V. mimicus* VM573 and exconjugants were selected on LB agar plates supplemented with 10 μg/ml chloramphenicol in the absence of DL-α,ε-diaminopimelic acid according to Demarre *et al.* [49].

Proteins purification and analysis

E. coli BL21(DE3) carrying p$acaDC^{6\times His}$ was grown to $OD_{600 \text{ nm}} = 0.5$ and induced for 2 hours with 1 mM of IPTG. Purification of AcaC tagged with a 6×His C-terminal epitope was done using a Ni-NTA affinity chromatography following the manufacturer's instructions (Qiagen). Migration of the purified proteins on 12% SDS-PAGE gel and Western blotting experiments using anti-6×His tag antibody were done as described by the manufacturer (Life Technologies/Invitrogen). Protein identification was performed at the proteomics platform of the Université de Sherbrooke on an excised acrylamide gel slice digested with trypsin and subjected to LC/MS/MS analysis as previously described [54].

ChIP-exo experiments and RNA sequencing

A thorough description of the chromatin immunoprecipitation coupled with exonuclease digestion and RNA sequencing procedures is given in Text S1 and Table S5.

RNA isolation and qRT-PCR

Cells from *V. mimicus* VM573 that contain no vector or p$acaCD$ were recovered after 2.5 hours of induction with 0.02% of arabinose. Total RNA extraction was done using an RNeasy minikit (Qiagen) following the manufacturer's instructions. Purified RNA samples were subsequently subjected to gDNA digestion using Turbo DNase (Ambion) following the manufacturer's instructions. RNA integrity was assessed using an Agilent 2100 Bioanalyzer (Agilent Technologies). qRT-PCR assays were performed on the RNomics platform of the Laboratoire de Génomique Fonctionnelle de l'Université de Sherbrooke (http://lgfus.ca). Reverse transcription was performed on 2.2 μg total RNA with Transcriptor reverse transcriptase, random hexamers, dNTPs (Roche Diagnostics), and 10 units of RNAseOUT (Invitrogen Life Technologies) following the manufacturer's protocol in a total volume of 20 μl. All forward and reverse primers were individually resuspended to 20–100 μM stock solutions in Tris-EDTA buffer (IDT) and diluted as a primer pair to 1 μM in RNase DNase-free water (IDT). Quantitative PCR (qPCR) reactions were performed in 10-μl volumes in 96 well plates on a CFX-96 thermocycler (Bio-Rad) with 5 μL of 2× iTaq Universal SYBR Green Supermix (Bio-Rad), 10 ng (3 μl) cDNA, and 200 nM final (2 μl) primer pair solutions. The following cycling conditions were used: 3 min at 95°C; 50 cycles: 15 s at 95°C, 30 s at 60°C, 30 s at 72°C. Relative expression levels of *int* (VMD_06510), VMD_06490, VMD_06480 and *xis* (VMD_06410) were calculated using a model taking into account multiple stably expressed reference genes [55] and housekeeping genes *rpoZ* and *gyrA* evaluated by geNorm [56]. Primer design (see Table S4) and validation were evaluated as described elsewhere [57]. In every qPCR run, a no-template control was performed for each primer pair and a no-reverse transcriptase control was performed for each cDNA preparation. Experiments were carried out three times on three biological replicates and combined.

Detection of SGI1 and MGIVmi1 excision

Excision of the GIs was detected by PCR on genomic DNA of the strains containing either SGI1 (*S. enterica* or *E. coli*) or MGIVmi1 (*V. mimicus*) using the primers listed in the Table S4. For SGI1, the *attL* site was amplified using primer pair SGI-1attL.for/SGI-1attL.rev in *S. enterica* and EcU7-L12.for/SGI-1attL.rev in *E. coli* [15]. The chromosomal site *attB* was detected using SGI-1attL.for/SGI-1attR.rev in *S. enterica* and EcU7-L12.for/Ec104D.rev in *E. coli*. The *attP* site carried by the extrachromosomal circular form of the element was amplified using the primer pair SGI-1attL.rev/SGI-1attR.for. Based on the same methodology for MGIVmi1 in *V. mimicus*, primer pairs GIVmi-A/GIVmi-B, GIVmi-A/GIVmi-D and GIVmi-B/GIVmi-C were used to detect *attL*, *attB* and *attP*, respectively.

Phylogenetic analyses

The molecular phylogenetic analysis of the $acr1$-$vcr147$-$acaDC$-$acr2$ locus was conducted in MEGA6 [58]. The nucleotide

sequence of the 2452-bp sequence of pVCR94 starting at the initiation codon of *acr1* and ending at the initiation codon of *acr2* was used to search for homologous sequences in the Genbank Nucleotide collection (nr/nt) database using Megablast [59]. Phylogenetic analyses were computed using a nucleotide alignment generated by MUSCLE [60]. The evolutionary history was inferred by using the Maximum Likelihood method. Initial tree(s) for the heuristic search were obtained automatically by applying Neighbor-Join and BioNJ algorithms to a matrix of pairwise distances estimated using the Maximum Composite Likelihood (MCL) approach, and then selecting the topology with superior log likelihood value. Identical procedures were used for the molecular phylogenetic analysis of the 1101-bp *repA* gene of pVCR94 (Figure S1).

Data availability

Fastq files for each experiment were deposited at the NCBI Sequence Read Archive (SRA) under accession numbers SRX675564 and SRR1544064 for ChIP-exo, SRX675582 and SRR1544143 for total RNAseq as well as SRX675814 and SRR1544479 for 5′-RACE. Complete data from aligned reads for ChIP-exo and RNA-seq can also be visualized using the UCSC genome browser at http://bioinfo.ccs.usherbrooke.ca/pVCR94.html.

Supporting Information

Figure S1 Molecular phylogenetic analysis of the *repA* replication initiation gene by Maximum Likelihood method. The evolutionary history was inferred by using the Maximum Likelihood method based on the Hasegawa-Kishino-Yano model [67]. The tree with the highest log likelihood (−2386.8588) is shown. The percentage of trees in which the associated taxa clustered together is shown next to the branches. A discrete Gamma distribution was used to model evolutionary rate differences among sites (5 categories (+G, parameter = 0.2014)). The tree is drawn to scale, with branch lengths measured in the number of substitutions per site. The analysis involved 45 nucleotide sequences. Codon positions included were 1st+2nd+3rd+Noncoding. There were a total of 1101 positions in the final dataset. Evolutionary analyses were conducted in MEGA6 [58]. The background color of each leaf indicates the original host species from which each plasmid was isolated. *, XNC1_p lacks the *acr1-vcrx147-acaDC-acr2* regulation cluster.
(TIF)

Figure S2 The 3×FLAG epitope does not alter the function of AcaCD. The donor strain *E. coli* MG1655 Rf was used to transfer pVCR94ΔX or its Δ*acaDC* mutant (Su Sp) to the recipient strain MG1655 Nx. AcaCD and SetCD complementation assays were carried out with the native D subunit and the C subunit C-terminally fused to the 3×FLAG epitope expressed from an IPTG-inducible promoter (P_{tac}) provided by pAH56, i.e. p*acaDC*$^{3×FLAG}$ (*acaDC*$^{3×FLAG}$), p*setDC*$^{3×FLAG}$ (*setDC*$^{3×FLAG}$) or empty pAH56 (0) integrated into the *attB*$_\lambda$ locus. Exconjugants were selected as Nx Su Sp colonies. The bars represent the mean and standard deviation values obtained from at least 3 biological replicates. The asterisks indicate that the frequency of transfer was below the limit of detection ($<10^{-8}$).
(TIF)

Figure S3 Comparison of the genetic context of genes coding for AcaCD and SetCD orthologs in IncA/C plasmids and SXT/ R391 ICEs. Schematic representation of regulatory regions of

pVCR94 from *V. cholerae* O1 El Tor (NC_023291.1) and SXT from *V. cholerae* O139 (AY055428.1). Arrows of similar color represent genes predicted to have similar functions: green, transcriptional activator; yellow, putative transcriptional regulator; red, transcriptional repressor; blue, conjugative transfer; light blue, putative lytic transglycosylase; orange, replication; black, site-specific recombination; white, unknown function. Blue stars indicate the position of origins of transfer (*oriT*). The orange star indicates the position of the origin of replication (*oriV*) of pVCR94 based on identity with pRA1 from *Aeromonas hydrophila* (NC_012885). The black star indicates the position of the *attP* site for chromosomal integration of SXT by site-specific recombination. The percent of identity of orthologous proteins are indicated on dashed lines.
(TIF)

Figure S4 Alignment of AcaCD-dependent promoters in pVCR94. The AcaCD motif is as represented in Figure 3C. AcaCD boxes obtained by MAST analysis are shown in bold green capital letters with their respective *p*-value and downstream regulated gene. The positions of the transcription start sites obtained from 5′-RACE data are indicated in bold blue capital letters and underlined (TSS). Shine-Dalgarno sequences (SD) are underlined while start codons are in capital letters. The approximate positions of the −35 and −10 regions are highlighted in gray. The length of spacers between the represented transcription start sites and the Shine-Dalgarno regions is indicated in base pairs. Since no clear 5′-RACE signal was observed for *vcrx035* and *vcrx098*, the approximate positions of expected transcription start sites are underlined and shown in bold black capital letters.
(TIF)

Table S1 Open reading frames (ORFs) of pVCR94 coding for putative transcriptional regulators.
(DOCX)

Table S2 *acr1-vcrx147-acaDC-acr2* orthologous clusters in IncA/C plasmids.
(DOCX)

Table S3 AcaCD-regulated promoters identified by ChIP-exo and 5′-RACE.
(DOCX)

Table S4 Primers used in this study.
(DOCX)

Table S5 Illumina libraries sequenced in this study.
(DOCX)

Dataset S1 RNAseq transcriptome profiling of wild-type pVCR94, pVCR94Δ*acaDC* and complemented pVCR94Δ*acaCD*.
(XLS)

Text S1 Additional experimental procedures.
(DOCX)

Author Contributions

References

1. WHO (2014) Antimicrobial resistance: global report on surveillance. World Health Organization. pp. 257.
2. Johnson TJ, Lang KS (2012) IncA/C plasmids: An emerging threat to human and animal health? Mob Genet Elements 2: 55–58.
3. Aoki T, Egusa S, Kimura T, Watanabe T (1971) Detection of R factors in naturally occurring Aeromonas salmonicida strains. Appl Microbiol 22: 716–717.
4. Wantanabe T, Aoki T, Ogata Y, Egusa S (1971) Anbtibiotics and drug resistance in animals. R factors related to fish culturing. Ann N Y Acad Sci 182: 383–410.
5. Walsh TR, Weeks J, Livermore DM, Toleman MA (2011) Dissemination of NDM-1 positive bacteria in the New Delhi environment and its implications for human health: an environmental point prevalence study. Lancet Infect Dis 11: 355–362.
6. Peirano G, Ahmed-Bentley J, Fuller J, Rubin JE, Pitout JD (2014) Travel-related carbapenemase-producing Gram-negative bacteria in Alberta, Canada: the first 3 years. J Clin Microbiol 52: 1575–1581.
7. Rahman M, Shukla SK, Prasad KN, Ovejero CM, Pati BK, et al. (2014) Prevalence and molecular characterisation of New Delhi metallo-beta-lactamases NDM-1, NDM-5, NDM-6 and NDM-7 in multidrug-resistant Enterobacteriaceae from India. Int J Antimicrob Agents: 30–7.
8. Dortet L, Poirel L, Nordmann P (2014) Worldwide dissemination of the NDM-type carbapenemases in Gram-negative bacteria. Biomed Res Int 2014: doi:10.1155/2014/249856
9. Fricke WF, Welch TJ, McDermott PF, Mammel MK, LeClerc JE, et al. (2009) Comparative genomics of the IncA/C multidrug resistance plasmid family. J Bacteriol 191: 4750–4757.
10. Welch TJ, Fricke WF, McDermott PF, White DG, Rosso ML, et al. (2007) Multiple antimicrobial resistance in plague: an emerging public health risk. PLoS One 2: e309.
11. Lindsey RL, Frye JG, Fedorka-Cray PJ, Meinersmann RJ (2011) Microarray-based analysis of IncA/C plasmid-associated genes from multidrug-resistant Salmonella enterica. Appl Environ Microbiol 77: 6991–6999.
12. Folster JP, Pecic G, McCullough A, Rickert R, Whichard JM (2011) Characterization of bla(CMY)-encoding plasmids among Salmonella isolated in the United States in 2007. Foodborne Pathog Dis 8: 1289–1294.
13. Arpin C, Thabet L, Yassine H, Messadi AA, Boukadida J, et al. (2012) Evolution of an incompatibility group IncA/C plasmid harboring bla_{CMY-16} and $qnrA6$ genes and its transfer through three clones of Providencia stuartii during a two-year outbreak in a Tunisian burn unit. Antimicrob Agents Chemother 56: 1342–1349.
14. Douard G, Praud K, Cloeckaert A, Doublet B (2010) The Salmonella genomic island 1 is specifically mobilized in trans by the IncA/C multidrug resistance plasmid family. PLoS One 5: e15302.
15. Doublet B, Boyd D, Mulvey MR, Cloeckaert A (2005) The Salmonella genomic island 1 is an integrative mobilizable element. Mol Microbiol 55: 1911–1924.
16. Mulvey MR, Boyd DA, Olson AB, Doublet B, Cloeckaert A (2006) The genetics of Salmonella genomic island 1. Microbes Infect 8: 1915–1922.
17. Hall RM (2010) Salmonella genomic islands and antibiotic resistance in Salmonella enterica. Future Microbiol 5: 1525–1538.
18. Fernandez-Alarcon C, Singer RS, Johnson TJ (2011) Comparative genomics of multidrug resistance-encoding IncA/C plasmids from commensal and pathogenic Escherichia coli from multiple animal sources. PLoS One 6: e23415.
19. Carraro N, Sauve M, Matteau D, Lauzon G, Rodrigue S, et al. (2014) Development of pVCR94ΔX from Vibrio cholerae, a prototype for studying multidrug resistant IncA/C conjugative plasmids. Front Microbiol 5: 44.
20. Wozniak RA, Fouts DE, Spagnoletti M, Colombo MM, Ceccarelli D, et al. (2009) Comparative ICE genomics: insights into the evolution of the SXT/R391 family of ICEs. PLoS Genet 5: e1000786.
21. Allen KJ, Poppe C (2002) Occurrence and characterization of resistance to extended-spectrum cephalosporins mediated by beta-lactamase CMY-2 in Salmonella isolated from food-producing animals in Canada. Can J Vet Res 66: 137–144.
22. Call DR, Singer RS, Meng D, Broschat SL, Orfe LH, et al. (2010) bla_{CMY-2}-positive IncA/C plasmids from Escherichia coli and Salmonella enterica are a distinct component of a larger lineage of plasmids. Antimicrob Agents Chemother 54: 590–596.
23. Han J, Lynne AM, David DE, Nayak R, Foley SL (2012) Sequencing of plasmids from a multi-antimicrobial resistant Salmonella enterica serovar Dublin strain. Food Research International 45: 931–934.
24. Cooper KK, Mandrell RE, Louie JW, Korlach J, Clark TA, et al. (2014) Complete Genome Sequences of Two Escherichia coli O145:H28 Outbreak Strains of Food Origin. Genome Announc 2. doi: 10.1128/genomeA.00482-14
25. Liu X, Matsumura P (1994) The FlhD/FlhC complex, a transcriptional activator of the Escherichia coli flagellar class II operons. J Bacteriol 176: 7345–7351.
26. Fernandez-Lopez R, Del Campo I, Revilla C, Cuevas A, de la Cruz F (2014) Negative feedback and transcriptional overshooting in a regulatory network for horizontal gene transfer. PLoS Genet 10: e1004171.
27. Doyle M, Fookes M, Ivens A, Mangan MW, Wain J, et al. (2007) An H-NS-like stealth protein aids horizontal DNA transmission in bacteria. Science 315: 251–252.
28. Hochhut B, Waldor MK (1999) Site-specific integration of the conjugal Vibrio cholerae SXT element into prfC. Mol Microbiol 32: 99–110.
29. Beaber JW, Hochhut B, Waldor MK (2002) Genomic and functional analyses of SXT, an integrating antibiotic resistance gene transfer element derived from Vibrio cholerae. J Bacteriol 184: 4259–4269.
30. Beaber JW, Hochhut B, Waldor MK (2004) SOS response promotes horizontal dissemination of antibiotic resistance genes. Nature 427: 72–74.
31. Rhee HS, Pugh BF (2012) ChIP-exo method for identifying genomic location of DNA-binding proteins with near-single-nucleotide accuracy. Curr Protoc Mol Biol: doi: 10.1002/0471142727.mb2124s100
32. Bailey TL, Elkan C (1994) Fitting a mixture model by expectation maximization to discover motifs in biopolymers. Proc Int Conf Intell Syst Mol Biol 2: 28–36.
33. Bailey TL, Gribskov M (1998) Combining evidence using p-values: application to sequence homology searches. Bioinformatics 14: 48–54.
34. Browning DF, Busby SJ (2004) The regulation of bacterial transcription initiation. Nat Rev Microbiol 2: 57–65.
35. Lang KS, Danzeisen JL, Xu W, Johnson TJ (2012) Transcriptome mapping of pAR060302, a bla_{CMY-2}-positive broad-host-range IncA/C plasmid. Appl Environ Microbiol 78: 3379–3386.
36. Kiss J, Nagy B, Olasz F (2012) Stability, entrapment and variant formation of Salmonella genomic island 1. PLoS One 7: e32497.
37. Boyd DA, Shi X, Hu QH, Ng LK, Doublet B, et al. (2008) Salmonella genomic island 1 (SGI1), variant SGI1-I, and new variant SGI1-O in Proteus mirabilis clinical and food isolates from China. Antimicrob Agents Chemother 52: 340–344.
38. Daccord A, Ceccarelli D, Burrus V (2010) Integrating conjugative elements of the SXT/R391 family trigger the excision and drive the mobilization of a new class of Vibrio genomic islands. Mol Microbiol 78: 576–588.
39. Daccord A, Mursell M, Poulin-Laprade D, Burrus V (2012) Dynamics of the SetCD-regulated integration and excision of genomic islands mobilized by integrating conjugative elements of the SXT/R391 family. J Bacteriol 194: 5794–5802.
40. Bellanger X, Payot S, Leblond-Bourget N, Guedon G (2014) Conjugative and mobilizable genomic islands in bacteria: evolution and diversity. FEMS Microbiol Rev 38: 720–760.
41. Daccord A, Ceccarelli D, Rodrigue S, Burrus V (2013) Comparative analysis of mobilizable genomic islands. J Bacteriol 195: 606–614.
42. Quiles-Puchalt N, Carpena N, Alonso JC, Novick RP, Marina A, et al. (2014) Staphylococcal pathogenicity island DNA packaging system involving cos-site packaging and phage-encoded HNH endonucleases. Proc Natl Acad Sci U S A 111: 6016–6021.
43. Dower WJ, Miller JF, Ragsdale CW (1988) High efficiency transformation of E. coli by high voltage electroporation. Nucleic Acids Res 16: 6127–6145.
44. Occhino DA, Wyckoff EE, Henderson DP, Wrona TJ, Payne SM (1998) Vibrio cholerae iron transport: haem transport genes are linked to one of two sets of tonB, exbB, exbD genes. Mol Microbiol 29: 1493–1507.
45. Guzman LM, Belin D, Carson MJ, Beckwith J (1995) Tight regulation, modulation, and high-level expression by vectors containing the arabinose P_{BAD} promoter. J Bacteriol 177: 4121–4130.
46. Gibson DG (2011) Enzymatic assembly of overlapping DNA fragments. Methods Enzymol 498: 349–361.
47. Zeghouf M, Li J, Butland G, Borkowska A, Canadien V, et al. (2004) Sequential Peptide Affinity (SPA) system for the identification of mammalian and bacterial protein complexes. J Proteome Res 3: 463–468.
48. Haldimann A, Wanner BL (2001) Conditional-replication, integration, excision, and retrieval plasmid-host systems for gene structure-function studies of bacteria. J Bacteriol 183: 6384–6393.
49. Demarre G, Guerout AM, Matsumoto-Mashimo C, Rowe-Magnus DA, Marliere P, et al. (2005) A new family of mobilizable suicide plasmids based on broad host range R388 plasmid (IncW) and RP4 plasmid (IncPalpha) conjugative machineries and their cognate Escherichia coli host strains. Res Microbiol 156: 245–255.
50. Datsenko KA, Wanner BL (2000) One-step inactivation of chromosomal genes in Escherichia coli K-12 using PCR products. Proc Natl Acad Sci U S A 97: 6640–6645.
51. Ceccarelli D, Daccord A, Rene M, Burrus V (2008) Identification of the origin of transfer (oriT) and a new gene required for mobilization of the SXT/R391 family of integrating conjugative elements. J Bacteriol 190: 5328–5338.
52. Datta S, Costantino N, Court DL (2006) A set of recombineering plasmids for gram-negative bacteria. Gene 379: 109–115.
53. Cherepanov PP, Wackernagel W (1995) Gene disruption in Escherichia coli: TcR and KmR cassettes with the option of Flp-catalyzed excision of the antibiotic-resistance determinant. Gene 158: 9–14.

54. Boisvert FM, Ahmad Y, Gierlinski M, Charriere F, Lamont D, et al. (2012) A quantitative spatial proteomics analysis of proteome turnover in human cells. Mol Cell Proteomics 11: M111 011429.

55. Hellemans J, Mortier G, De Paepe A, Speleman F, Vandesompele J (2007) qBase relative quantification framework and software for management and automated analysis of real-time quantitative PCR data. Genome Biol 8: R19.

56. Vandesompele J, De Preter K, Pattyn F, Poppe B, Van Roy N, et al. (2002) Accurate normalization of real-time quantitative RT-PCR data by geometric averaging of multiple internal control genes. Genome Biol 3: RESEARCH0034.

57. Brosseau JP, Lucier JF, Lapointe E, Durand M, Gendron D, et al. (2010) High-throughput quantification of splicing isoforms. RNA 16: 442–449.

58. Tamura K, Stecher G, Peterson D, Filipski A, Kumar S (2013) MEGA6: Molecular Evolutionary Genetics Analysis version 6.0. Mol Biol Evol 30: 2725–2729.

59. Zhang Z, Schwartz S, Wagner L, Miller W (2000) A greedy algorithm for aligning DNA sequences. J Comput Biol 7: 203–214.

60. Edgar RC (2004) MUSCLE: multiple sequence alignment with high accuracy and high throughput. Nucleic Acids Res 32: 1792–1797.

61. Kimura M (1980) A simple method for estimating evolutionary rates of base substitutions through comparative studies of nucleotide sequences. J Mol Evol 16: 111–120.

62. Tamamura Y, Tanaka K, Akiba M, Kanno T, Hatama S, et al. (2013) Complete nucleotide sequences of virulence-resistance plasmids carried by emerging multidrug-resistant *Salmonella enterica* Serovar Typhimurium isolated from cattle in Hokkaido, Japan. PLoS One 8: e77644.

63. Zhang Y, Liu T, Meyer CA, Eeckhoute J, Johnson DS, et al. (2008) Model-based analysis of ChIP-Seq (MACS). Genome Biol 9: R137.

64. Bailey TL, Boden M, Buske FA, Frith M, Grant CE, et al. (2009) MEME SUITE: tools for motif discovery and searching. Nucleic Acids Res 37: W202–208.

65. McClure R, Balasubramanian D, Sun Y, Bobrovskyy M, Sumby P, et al. (2013) Computational analysis of bacterial RNA-Seq data. Nucleic Acids Res 41: e140.

66. Coulombe C, Poitras C, Nordell-Markovits A, Brunelle M, Lavoie MA, et al. (2014) VAP: a versatile aggregate profiler for efficient genome-wide data representation and discovery. Nucleic Acids Res 42: W485–W493.

67. Hasegawa M, Kishino H, Yano T (1985) Dating of the human-ape splitting by a molecular clock of mitochondrial DNA. J Mol Evol 22: 160–174.

68. Thompson CC, Vicente AC, Souza RC, Vasconcelos AT, Vesth T, et al. (2009) Genomic taxonomy of Vibrios. BMC Evol Biol 9: 258.

69. Garriss G, Poulin-Laprade D, Burrus V (2013) DNA-damaging agents induce the RecA-independent homologous recombination functions of integrating conjugative elements of the SXT/R391 family. J Bacteriol 195: 1991–2003.

70. Haldimann A, Wanner BL (2001) Conditional-replication, integration, excision, and retrieval plasmid-host systems for gene structure-function studies of bacteria. J Bacteriol 183: 6384–6393.